Online ISSN 2755-2500
Print ISSN 2755-2608
Volume 3 Number 2
March 2025
rsc.li/icm

Industrial Chemistry & Materials

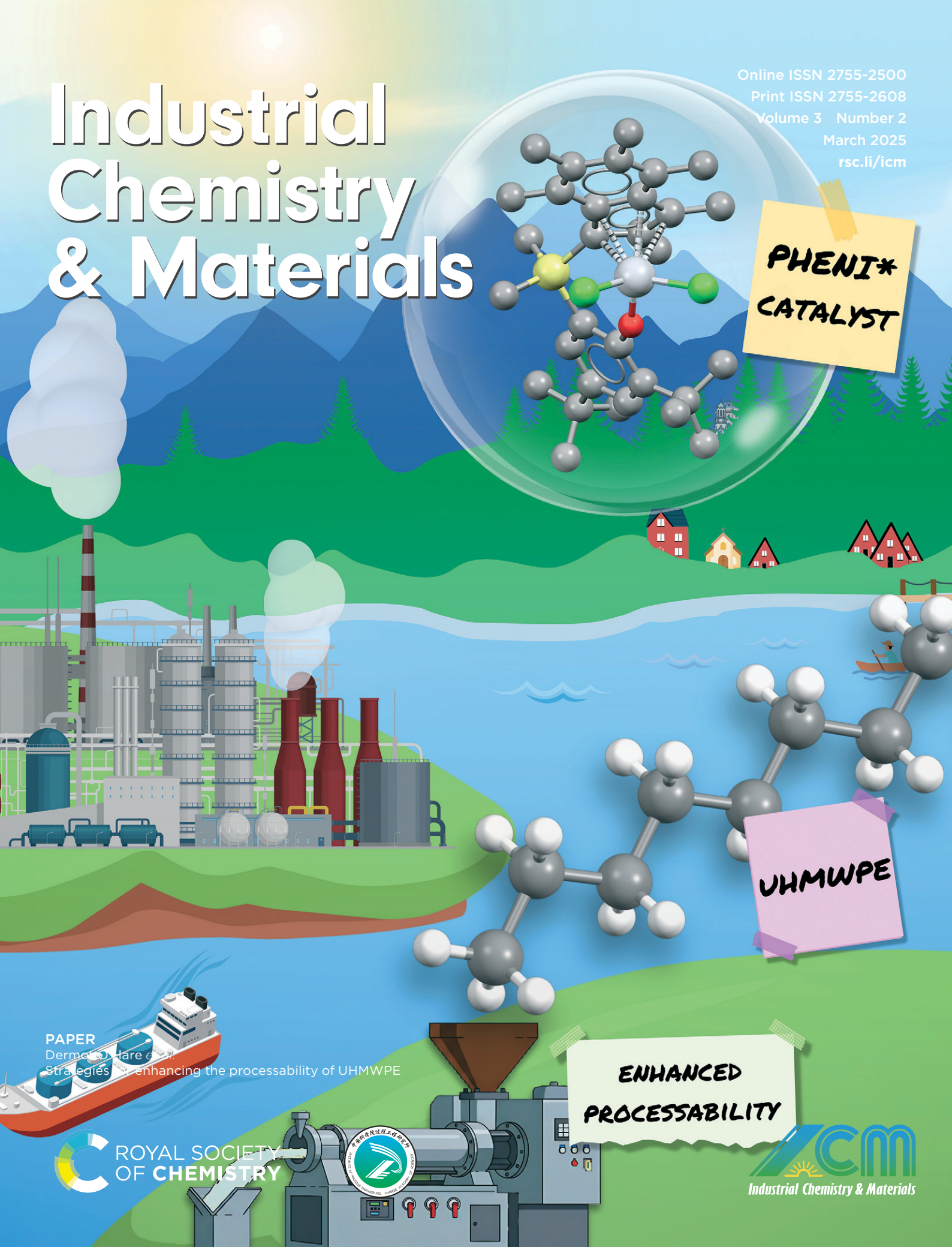

PAPER
Dermot O'Hare *et al.*
Strategies for enhancing the processability of UHMWPE

ROYAL SOCIETY OF CHEMISTRY

ICM
Industrial Chemistry & Materials

Industrial Chemistry & Materials

ROYAL SOCIETY OF CHEMISTRY

PAPER

View Article Online
View Journal | View Issue

Cite this: *Ind. Chem. Mater.*, 2025, **3**, 178

Strategies for enhancing the processability of UHMWPE†

Clement G. Collins Rice, [ab] Alexander Evans, [a] Zoë R. Turner, [a] Jirut Wattoom[bc] and Dermot O'Hare *[a]

Ultra-high molecular weight polyethylene (UHMWPE, $M_w > 10^6$ g mol^{-1}) has been prepared using slurry-phase titanium permethylindenyl-phenoxy (PHENI*) catalysts. Four strategies have been investigated for improving the melt processability of UHMWPE, which is the chief limiting factor to the applications of this high-performance polymer. 1) Active site engineering was used to explore the entanglement density in the resulting polymer, with substantially disentangled PE identified through thermal and rheological characterisation. 2) Hydrogen and $ZnEt_2$ were employed as chain transfer agents to modulate the polyethylene molecular weight and distribution (MWD). A sequential reactivity protocol using $ZnEt_2$ was able to produce bimodal UHMWPE with improved processability. 3) MWD tuning was further investigated using multisite catalysts, with the reaction conditions and Ti : Zr ratio able to control MWD to essentially arbitrary shapes. The inclusion of low molecular weight fractions into UHMWPE improves the processability without compromising mechanical characteristics. 4) Polymer-reinforced composite blends of UHMWPE with either HDPE or LDPE as a highly processable matrix were extruded and explored, with polymer miscibility and mechanical properties studied in detail.

Received 19th August 2024,
Accepted 4th October 2024

DOI: 10.1039/d4im00104d

rsc.li/icm

Keywords: Ultra-high molecular weight polyethylene; Processability; Molecular weight distribution; Polymer composites; Chain transfer agents.

1 Introduction

Ultra-high molecular weight polyethylene (UHMWPE), defined by a molecular weight in the millions of Daltons, is a specialty grade of PE considered an important engineering plastic due to its desirable properties. UHMWPE has a tensile strength and impact resistance unmatched among polymers and more comparable to steel.[1–3] It is chemically and abrasion resistant while also having a very low coefficient of friction, comparable to PTFE and described as self-lubricating.[4–7] Numerous applications exist for UHMWPE in the biomedical,[8] maritime, aerospace,[9] and ballistics sectors.[10,11] Outstanding performance is offered for total joint arthroplasty,[8,12–14] and UHMWPE is widely used as a bulletproof material.[10,15] Furthermore, UHMWPE may be melt- or gel-spun into fibres and woven into ropes and fabrics with extremely high toughness, higher strengths than *para*-amid fibres such as Kevlar®, and comparable properties to carbon fibre.[9,16–18] Composite materials, including monomaterials such as UHMWPE-reinforced HDPE are of growing interest with useful intrinsic properties and applications such as in aircraft and space structures.[19–22]

A feature of the extended chain length of UHMWPE macromolecules is their tendency to form interpenetrated networks of entanglements; UHMWPE is generally synthesised in processes where the rate of chain growth is greater than that of chain crystallisation, resulting in a large entanglement density in the amorphous region.[23,24] The entanglements act as physical crosslinks and profoundly influence the physical and mechanical properties of the semicrystalline polymer such as deformation behaviour.[25] The melt viscosity is highly dependent on molar mass and scales according to $\eta_0 \propto M^{3.4}$.[26] Entanglements and slow chain diffusion contribute to the extremely high melt viscosity of UHMWPE (comparable to the famous pitch drop experiment)[27] and renders it challenging to process, with common thermoplastic techniques like injection moulding impractical.[3] To circumvent this, the synthesis of substantially disentangled UHMWPE, which can be processed in the solid-state below the melting point,[28] and the production of polymer blends incorporating UHMWPE into a processable matrix have both been developed.[29,30] The production of nascently disentangled UHMWPE has been

[a] *Chemistry Research Laboratory, University of Oxford Department of Chemistry, 12 Mansfield Road, Oxford, OX1 3TA, UK. E-mail: dermot.ohare@chem.ox.ac.uk*
[b] *SENFI UK Ltd., Centre of Innovation and Enterprise, Begbroke Science Park, Woodstock Road, Begbroke, OX5 1PF, UK*
[c] *SCG Chemicals PLC, 1 Siam Cement Road, Bangsue, Bangkok 10800, Thailand*
† Electronic supplementary information (ESI) available: Polymerisation data and polymer characterisation data. See DOI: https://doi.org/10.1039/d4im00104d

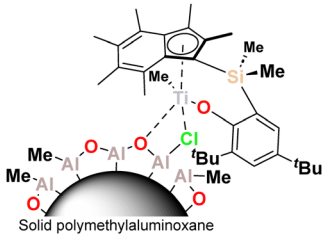

Fig. 1 Schematic structure of sMAO-supported PHENI* catalyst **1**.

pursued through engineering heterogeneous catalysts with spatially diluted active sites,[31–33] selective reduction of active sites,[34] and nitrogen microbubbles,[35,36] as well as the development of specific single-site molecular catalysts.[11,37–42] The formation of interfacial entanglements has been exploited to enhance polymer welding and UHMWPE recycling.[43]

The molecular weight and molecular weight distribution (MWD) of polyethylene have critical roles in the mechanical, rheological, and morphological properties.[44] Generally, high molecular weight PE possesses increased toughness and strength which is desirable in many applications.[45] The dispersion and shape of the molecular weight distribution are parameters which also influence the properties of polyolefin materials.[46] MWD can be tuned through polymer blending,[47] bifunctional catalysts,[30,45,48,49] sequential reactivity,[50] and catalyst support composition.[51]

In this work, four strategies are explored for enhancing the melt processability of UHMWPE. 1) The synthesis and characterisation of low entanglement UHMWPE is investigated using a slurry-phase titanium permethylindenyl-phenoxy (PHENI*) catalyst. Subsequently, the use of 2) chain transfer agents, 3) multisite catalysts and nanostructured reactor blends, and 4) polymer-reinforced polymer composites are reported all with the aim of producing polyethylene materials combining the mechanical properties of UHMWPE with the processability of conventional HDPE.

2 Results and discussion

The permethylindenyl-phenoxy (PHENI*) complex ^{Me_2}SB(^{tBu_2}ArO, I*)TiCl$_2$ ({(η^5-C$_9$Me$_6$)SiMe$_2$(2,4-^{t}Bu$_2$-C$_6$H$_2$O)}TiCl$_2$, **1**; I* = η^5-C$_9$Me$_6$) was synthesised according to established literature procedures and immobilised on solid polymethylaluminoxane (sMAO; [Al$_{sMAO}$]/[Ti] ∈ {100, 200, 400, 800}) to afford the solid catalysts **1**$_{sMAO(100–800)}$ (Fig. 1).[52–54] A preliminary discussion of the ethylene polymerisation characteristics of the heterogenised PHENI* catalyst system has been reported.[52] Detailed polymer characterisation is discussed in the ESI.†

2.1 Effect of catalyst surface concentration on entanglement density

The catalysts **1**$_{sMAO(100–800)}$ were used to polymerise ethylene for 30 minutes at 2 bar and 60 °C in 150 mL Rotaflo® ampoules containing 50 mL hexanes as diluent and 150 mg tri*iso*butylaluminium (TIBA; Table 1). The resulting polymers had weight-average molecular weight (M_w) in the range 2.1–2.9 MDa ($Đ$ = 3.7–5.2; Fig. S16†) as measured by gel-permeation chromatography (GPC). Polymerisation activity increased with [Al$_{sMAO}$]/[Ti] up to 7763 kg$_{PE}$ mol$_{Ti}^{-1}$ h^{-1} bar^{-1} for **1**$_{sMAO(800)}$. However, a decrease in gravimetric productivity reflects the increasing proportion of the support. Optimal productivity (1.06 kg$_{PE}$ g$_{cat.}^{-1}$ h^{-1}) was observed for [Al$_{sMAO}$]/[Ti] = 200. Polymer molecular weight appears to depend on the mass of solid catalyst, with M_w decreasing and dispersity ($Đ$) increasing as $m_{cat.}$ increases. This indicates an increase in the rate of chain transfer to relative to propagation and presumably results from aluminium in the support acting as a chain transfer agent.

Increasing the spatial dilution of active sites on the sMAO surface was anticipated to decrease the entanglement density since the probability of chain crystallisation occurring before entanglement formation is increased.[31–33] In all cases, analysis by differential scanning calorimetry (DSC) shows a decrease in both melting temperature (T_m) and crystallinity (X_c) in the second cycle compared to the nascent powder, consistent with recrystallisation being considerably impeded by re-entanglement in the melt (Fig. S17†).[55] The reduction in T_m from 144 °C (nascent) to 136 °C (melt-crystallised) is related to a reduction in crystallite thickness according to the Gibbs–Thomson equation and is consistent with increasing entanglement in the amorphous domain and therefore a low entanglement density in the nascent polymer.[56]

To assess this further, the polymers were subjected to a DSC annealing protocol,[28] and time-domain melt rheometry (Fig. 2 and S18–S22†).[57,58] The increase in storage modulus

Table 1 Polymerisation conditions: 2 bar ethylene, 150 mg TIBA, 50 mL hexanes, 60 °C, and 30 minutes

Run	[Al]/[Ti]^a	$m_{cat.}$ (mg)	n_{Ti} (μmol)	A^b	P^c	$M_w{}^d$ (MDa)	$Đ^d$
1	100	9.9	1.31	1670	0.88	2.47	3.8
2	200	9.9	0.71	3720	1.06	2.09	5.2
3	400	9.5	0.34	5560	0.78	2.59	4.3
4	800	9.3	0.17	7760	0.58	2.88	3.7
5	100	5.0	0.66	1930	0.96	3.03	3.6
6	400	19.5	0.69	4900	0.70	2.08	6.7
7	800	39.7	0.71	6070	0.22	1.69	6.5

^{a} [Al$_{sMAO}$]$_0$/[Ti]$_0$. ^{b} Activity /kg$_{PE}$ mol$_{Ti}^{-1}$ h^{-1} bar^{-1}. ^{c} Productivity /kg$_{PE}$ g$_{cat.}^{-1}$ h^{-1}. ^{d} Determined by GPC.

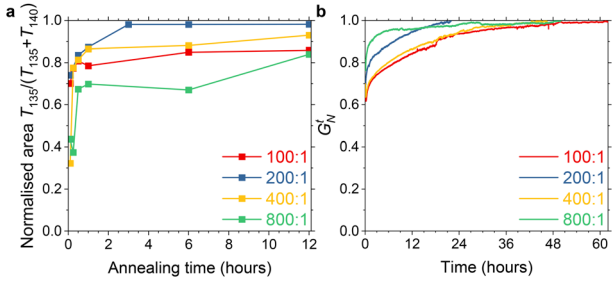

Fig. 2 (a) Normalised area $T_{135°C}/(T_{135°C} + T_{140°C})$ as a function of annealing time, and (b) normalised storage modulus (G'_N, measured at 160 °C, ω = 10 rad s^{-1}) as a function of time of polyethylene synthesised by $\mathbf{1}_{sMAO}$ of varying $[Al_{sMAO}]/[Ti]$.

(G') as a function of time – consistent with the formation of the equilibrium entangled state[23] – is essentially identical for $[Al_{sMAO}]/[Ti]$ = 100, 200, and 400, reaching a plateau modulus around 0.5 MPa after 40 h. Similarly, little difference is seen by thermal annealing, with 80% of the low-melting peak present after annealing for 30 minutes as a result of sequential chain detachment.[59] The $\mathbf{1}_{sMAO(800)}$ sample shows a slightly different profile, presumably due to the strong molecular weight dependence of these methods, but nonetheless G' build-up and rapid annealing are observed. This is consistent with the formation of low-entangled UHMWPE and suggests that below a critical surface concentration (at least 1% coverage) further decreasing the entanglement concentration may not be achievable by this method.

2.2 Chain transfer agents as a means of modulating MWD

Chain transfer agents (CTAs) can be used to modulate polymer molecular weight and molecular weight distribution (MWD).[60–63] The addition of molecular dihydrogen to the polymerisation system is expected to reduce the molecular weight of the polymer by acting as a chain transfer agent, promoting hydrogenation of the growing polymeryl chain and increasing the rate of chain termination relative to propagation.[64–66] Slurry-phase polymerisation was performed using $\mathbf{1}_{sMAO(200)}$ and a monomer feed consisting of ethylene/hydrogen in a ratio of 98 : 2 (2 bar total pressure). High catalytic activities are maintained, up to 1770 kg_{PE} mol_{Ti}^{-1} h^{-1} bar^{-1} at 60 °C (Fig. S24†). The addition of hydrogen likely leads to catalyst deactivation by the formation of a dormant hydride or bimetallic catalytic resting state.[67–72] Decreased activity in the presence of hydrogen is commonly seen for group four metallocene catalysts such as Cp_2ZrCl_2,[67,69] though calculations have suggested that ethylene insertion of the zirconocene hydride formed by hydrogenolysis ought to be kinetically facile.[66] As expected, polymer molecular weights were significantly suppressed in the presence of 2% hydrogen, decreasing by as much as 96% compared to polymerisation in the absence of hydrogen. Molecular weights in the region of 85–110 kDa are reported with broadened dispersities in the range 4.5–9.5 (Fig. S26†). Broadened MWDs have been commonly observed with Ziegler–Natta and metallocene catalysts in the presence of hydrogen.[64,69,73–75] The relatively lower calculated energy barrier for hydrogen insertion compared to that of ethylene is consistent with the observed large reduction in M_w at relatively low concentrations of H_2.[66] Industrially prevalent zirconocenes such as Cp_2ZrCl_2 and $(EBI)ZrCl_2$ (EBI = 1,2-ethylenebis(1-indenyl)) are known to show similarly significant hydrogen responses, though in these cases producing low molecular weight PE and PE waxes.[67,69] The CGCI* catalyst, $^{Me_2}SB(^{tBu}N$, I*)$TiCl_2$, supported on sMAO, shows a slightly stronger hydrogen response than PHENI*, with polymer molecular weights decreasing from 2.7 MDa to 41 kDa at 1.6% H_2 concentration with a 27% decrease in activity.[76] Some *ansa* I* zirconocene complexes have shown remarkable stability towards H_2 and the production of ultra-low molecular weight PE waxes with $M_n < 5$ kDa.[77]

Zinc(II) compounds are also examples of effective CTAs that have been used to modulate the molecular weight of polymers produced by metallocene catalysts.[78,79] Diethyl zinc has been used in sequential reactivity protocols to further tune the MWD, leading to bimodal polyethylenes with

Table 2 Polymerisation conditions: 10 mg $\mathbf{1}_{sMAO(200)}$, 2 bar ethylene, 150 mg TIBA, 50 mL hexanes, 60 °C, and 30 minutes (t_1 = 0–20 minutes)

Run	$[Zn]_t/[Ti]_0$	t_1 (minutes)	A^a	$M_w{}^b$ (MDa)	$Đ^b$	$\lvert\eta^*\rvert^c$ (kPa s)
8	0	—	3720	2.09	5.2	279
9	10	15	3270	2.37	4.7	264
10	50	15	3110	2.31	5.4	249
11	100	15	3090	2.20	5.4	241
12	200	15	2870	2.09	6.0	239
13	300	15	2820	2.07	8.6	211
14	1000	15	2460	2.24	13.6	236
15	1000	0	51	0.08	14.0	*n.d.*
16	1000	1	660	0.31	23.3	22.7
17	1000	5	1380	0.83	21.8	77.7
18	1000	10	2150	0.87	10.8	91.4
19	1000	20	3130	0.92	3.8	104

[a] Activity /kg_{PE} mol_{Ti}^{-1} h^{-1} bar^{-1}. [b] Determined by GPC. [c] Measured at 160 °C, ω = 1 rad s^{-1}.

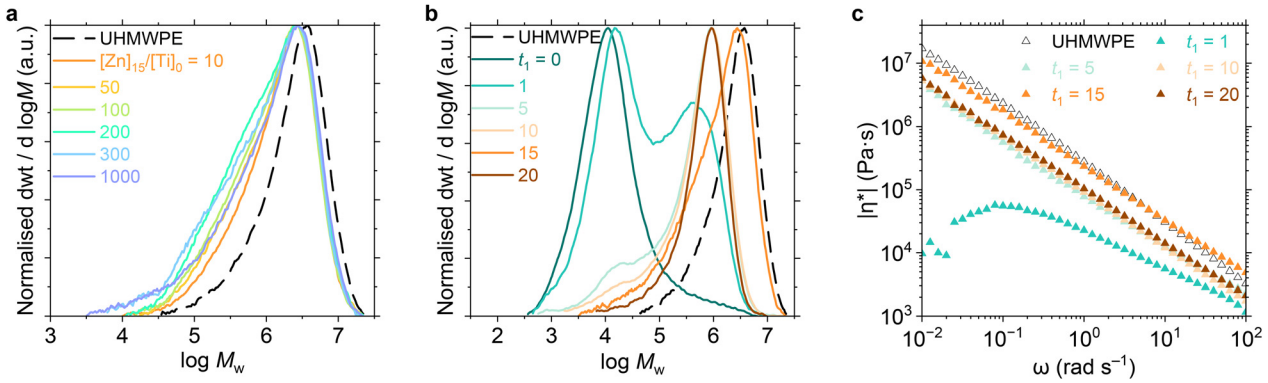

Fig. 3 (a and b) Gel-permeation chromatograms, and (c) rheological complex viscosity (SAOS frequency sweep measured at 160 °C) of polyethylene as a function of $[Zn]_{t_1}/[Ti]_0$ for polymerisation in the presence of $ZnEt_2$ ((a) t_1 = 15 minutes; (b and c) $[Zn]_{t_1}/[Ti]_0$ = 1000).

desirable melt processability and mechanical properties.[45,50,80] CTAs have also been successfully employed in chain shuttling copolymerisation to enable the production of olefin block copolymers, an emerging class of thermoplastic materials with highly desirable properties,[81–83] including as compatibilisers for post-consumer recycled plastic resins.[84]

$ZnEt_2$ ($[Zn]_{t_1}/[Ti]_0$ = 10–1000) was charged into a sidearm of the reaction ampoule and introduced to the reaction at t_1 = 15 minutes (Table 2; Fig. S27†). An interaction between $ZnEt_2$ and TIBA has been observed to result in the formation of hydride species and metallic zinc.[85] Polymerisation activity decreased as the loading of $ZnEt_2$ increased, and the M_w of the polymers was not found to be strongly affected. However, dispersity increased with increasing [Zn] corresponding to a decrease in M_n, from 402 kDa ($Đ$ = 5.2) in the absence of $ZnEt_2$ to 164 kDa ($Đ$ = 13.6) at [Zn]/[Ti] = 1000. Varying t_1 at a fixed $[Zn]_{t_1}/[Ti]_0$ = 1000 resulted in a more dramatic decrease in activity as t_1 decreased (660 kg_{PE} mol_{Ti}^{-1} h^{-1} bar^{-1} at t_1 = 1 minute) along with the formation of a metallic grey precipitate. The M_w decreases as t_1 decreases, to 305 kDa at t_1 = 1 minute, with dispersity increasing (Fig. S28 and S29†).

As a function of increasing [Zn]/[Ti], despite the broadened MWDs and decreased M_n, very little change was seen in the melt complex viscosity, η^*, as measured rheometrically, decreasing by at most 24% compared to UHMWPE produced without $ZnEt_2$ CTA (Fig. S30†). It is known that polymer rheology is highly sensitive to even small fractions of UHMW chains.[86] However, at short t_1 times, a significant reduction in η^* is observed – to 22.7 kPa s at t_1 = 1 minute, an order of magnitude reduced compared to the zinc-free control polymerisation and indicative of increased melt processability (Fig. 3). This is consistent with the greatly broadened MWDs in this case, with $Đ$ = 23.5 at t_1 = 1 minute, with a clear bimodal profile. DSC shows the presence of a single thermal phase at a slow heating rate of 1 K min^{-1}, with no evidence found of distinct HDPE and UHMWPE particles (Fig. S32†). Sequential reactivity is essential for the production of bimodal PE by this method: at t_1 = 0 minutes, monomodal low molecular weight (with a high M_w shoulder) PE is produced with low productivity (M_w = 83 kDa, $Đ$ = 14). The rapid propagation kinetics of PHENI* enable efficient production of UHMWPE in the first phase of the reaction even at low t_1 values. Through tuning [Zn] and t_1 essentially arbitrary MWDs are possible using the PHENI* catalyst system.

2.3 Multisite catalysts for the synthesis of all-polyolefin composites

Multisite catalysts were prepared by coimmobilising on sMAO complexes capable of producing polyethylenes with a range of molecular weights. In addition to the PHENI* complex for UHMWPE, *rac*-(EBI)$ZrCl_2$ (**2**) was used to produce conventional HDPE with M_w on the order of 10^5 g mol^{-1}. Typically, low molecular weight PE imparts stiffness and

Table 3 Polymerisation conditions: 10 mg solid catalyst, 2 bar ethylene, 150 mg TIBA, 50 mL hexanes, 60 °C, and 30 minutes

Run	Catalyst	A^a	$M_w{}^b$ (kDa)	$Đ^b$	$\lvert\eta^*\rvert^c$ (kPa s)	$\sigma_M{}^d$ (MPa)
20	$\mathbf{1}_{sMAO}$	3720	2090	5.2	280	*n.d.*
21	$\mathbf{2}_{sMAO}$	5540	134	3.4	20.4	13.9 ± 0.2
22	$(\mathbf{1}_9/\mathbf{2}_1)_{sMAO}$	3270	1067	5.3	234	16.2 ± 2.0
23	$(\mathbf{1}_3/\mathbf{2}_1)_{sMAO}$	4010	647	6.6	53.2	16.9 ± 1.7
24	$(\mathbf{1}_2/\mathbf{2}_1)_{sMAO}$	3850	763	6.2	73.8	17.6 ± 1.1
25	$(\mathbf{1}_1/\mathbf{2}_1)_{sMAO}$	3980	540	8.5	87.0	14.9 ± 2.5
26	$(\mathbf{1}_1/\mathbf{2}_2)_{sMAO}$	4270	397	6.7	54.3	16.7 ± 0.8
27	$\mathbf{1}_{sMAO}$ + $\mathbf{2}_{sMAO}$	4460	570	8.8	70.8	14.9 ± 1.4

[a] Activity /kg_{PE} mol_{Ti}^{-1} h^{-1} bar^{-1}. [b] Determined by GPC. [c] Measured at 160 °C, ω = 1 rad s^{-1}. [d] Ultimate tensile stress ($\mu \pm \sigma$).

processability, and (ultra) high molecular weight PE increases toughness and improves mechanical properties.[48] Ethylene polymerisations were performed with $(\mathbf{1}_n/\mathbf{2}_m)_{\mathbf{sMAO}}$ with varied Ti : Zr ratios ([Ti]/[Zr] = n/m = 0.5–9; [Al_{sMAO}]/[Ti + Zr] = 200), and with a 1 : 1 physical mixture ($\mathbf{1}_{\mathbf{sMAO}}$ + $\mathbf{2}_{\mathbf{sMAO}}$; Table 3). It had been anticipated that a coimmobilised multisite catalyst should result in a much more intimate reactor blend that a physical mixture of catalyst particles.[87–89] Since polymerisation activities, polymer molecular weights and dispersities are all dependent on the polymerisation temperature (T_p), polymerisations were performed using multisite catalysts at 50 ≤ T_p ≤ 90 °C. Approximately additive activities are observed compared to the individually immobilised catalysts, with little difference between coimmobilised and physical mixture catalysts (Fig. S33†) indicating little cooperativity but also no degradation in performance. At a DSC heating rate of 1 K min^{-1}, two distinct melting transitions are observed for the physical mixture catalyst suggestive of the heterogeneous melting of isolated UHMWPE and HDPE particles (Fig. S35†). By contrast, the coimmobilised catalysts all produce homogeneous polymers with a single thermal transition consistent with nanostructured polymers.

Gel-permeation chromatography was used to determine the molecular weight distributions of the polyethylenes synthesised by multisite catalysts (Fig. 4a and S36–S39; Table S8†). Bimodal PE of varying distribution is achieved, with $Đ$ up to 11.5 and the shape and location of the peaks being tunable as a function of the [Ti]/[Zr] ratio and the temperature of polymerisation. Under this regime, increasing T_p acts to lower the M_w of the two fractions (though more significantly for the high M_w fraction), and increases the productivity of **2** relative to **1**, skewing the MWDs towards lower M_w. Through this tunability, and the judicious selection of metallocenes, MWDs of essentially arbitrary form may be achieved. Analysis of the chromatograms shows that mass fractions as high as 78 wt% of UHMWPE can be achieved using $(\mathbf{1}_9/\mathbf{2}_1)_{\mathbf{sMAO}}$, far higher than could typically be achieved through compounding, highlighting an advantage of the reactor blend method.

The polymers produced at 60 °C by all multisite catalysts were analysed by melt rheology to assess processability, and by dynamic mechanical analysis (DMA) and tensile analysis (Fig. 4b and c and S40–S44†). From rheology, the melt viscosity, η^*, of bimodal PE is intermediate between the UHMWPE produced by $\mathbf{1}_{\mathbf{sMAO}}$ and the HDPE produced by $\mathbf{2}_{\mathbf{sMAO}}$, roughly in proportion to the weight of the two fractions in the MWD, meaning that broadening the MWD is found to increase the melt processability of the resulting polymer. Measured at 160 °C and an angular frequency, ω, of 1 rad s^{-1}, the viscosity of HDPE synthesised by $\mathbf{2}_{\mathbf{sMAO}}$ (20.4 kPa s) was an order of magnitude less than that of the UHMWPE produced by $\mathbf{1}_{\mathbf{sMAO}}$. The bimodal polymer produced with $(\mathbf{1}_1/\mathbf{2}_1)_{\mathbf{sMAO}}$ was measured to have a complex viscosity of 87.0 kPa s, intermediate between the UHMWPE and HDPE cases. Essentially no difference is seen between the coimmobilised and physical mixture catalysts due to rapid equilibration in the melt phase.

Small-scale mechanical characterisation presents challenges due to the influence of small imperfections that can act to concentrate stress. Despite this, clear trends can be observed through tensile strength testing and dynamic mechanical analysis (DMA) in relation to MWD tuning. Generally, the increasing high molecular weight fraction leads to increased tensile strength and decreased strain at break (ε_B). Notably, runs 23 and 24 resulted in materials which demonstrated greater tensile strengths (16.9 ± 1.7 and 17.3 ± 1.1 MPa respectively) and ε_B (830 ± 41 and 780 ± 100% respectively) than would be expected from a simple mixing law, indicative of a synergistic enhancement in the mechanical properties of nanostructured all-polyethylene composites.[89] This is mirrored in DMA (Fig. S41†) where the complex viscoelastic modulus E^* of runs 23 and 24 is decreased compared to neat UHMWPE or HDPE. The MWD dependence is evident in that runs 23 and 24 have high molecular weight fractions of 49.9 and 55.2 wt% respectively ($\log M > 5.5$) perhaps indicating a mechanically optimal composition.

Together this shows that multisite catalysts coimmobilised on sMAO are able to produce homogeneous nanostructured

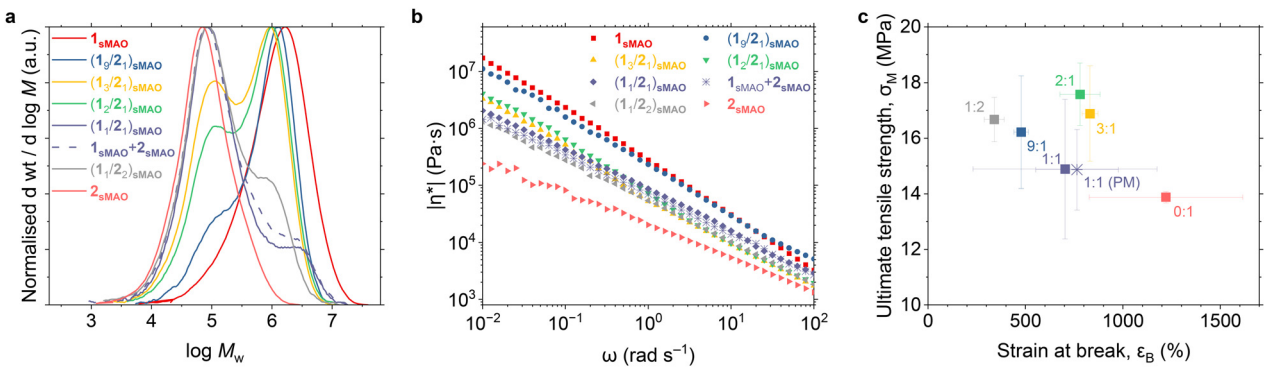

Fig. 4 (a) Gel-permeation chromatograms; (b) rheological complex viscosity (SAOS frequency sweep measured at 160 °C); (c) tensile results of polyethylene produced at T_p = 60 °C by coimmobilised multisite catalysts $(\mathbf{1}_n/\mathbf{2}_m)_{\mathbf{sMAO}}$ (or the physical mixture $\mathbf{1}_{\mathbf{sMAO}}$ + $\mathbf{2}_{\mathbf{sMAO}}$) as a function of [Ti]/[Zr].

polyethylenes with broad and tuneable MWDs and enhanced melt processability compared to pure UHMWPE while maintaining some of the mechanical properties of the pure material. A notable feature of the multisite strategy is the ability to produce PEs with MWDs that are inaccessible by polymer blending which is limited by the processability of raw UHMWPE and the solubility of UHMWPE in HDPE *vide infra*.[90] Furthermore, the PHENI* complex has proven to be an effective catalyst for producing the UHMW component in a PE reactor blend.

2.4 Self-reinforced polyethylene–polyethylene blends

The extremely high melt viscosity of UHMWPE motivates the exploration of polymer blends: using a lower molecular weight PE, to improve the melt flow index (MFI), blended with UHMWPE, to confer high-performance properties such as tensile strength and impact resistance. One important aspect of this is polyethylene–polyethylene miscibility, which has been the subject of extensive study, with somewhat contradictory conclusions. Chen *et al.* found inconsistencies between thermal and rheological measurements, and concluded that UHMWPE was miscible with LDPE but with neither HDPE nor LLDPE.[91,92] By contrast, Kyu *et al.* concluded that UHMWPE is miscible with HDPE, LDPE, and LLDPE in the melt but that only HDPE and LLDPE were able to co-crystallise with UHMWPE in the solid state.[93] It has been found that the branching content of polyethylenes is a major factor in determining miscibility.[94,95] Moreover, Tao *et al.* have recently shown that entanglement density greatly influenced the microstructure and mechanical properties of UHMWPE/HDPE blends, with the improved chain diffusion of weakly entangled UHMWPE conferring preferable reinforcing properties.[96] Disentanglement of UHMWPE has also been shown to increase dissolution in HDPE.[97] To explore this further, UHMWPE synthesised by a PHENI* catalyst was microcompounded with either a commercial LDPE (Sigma Aldrich; M_w = 89 kDa; $Đ$ = 8.5; MFI = 25 g/10 min (190 °C, 2.16 kg)), or HDPE (SCG Chemicals PLC; M_w = 225 kDa; $Đ$ = 25; MFI = 15.7 g/10 min (190 °C, 2.16 kg)) and extruded into ribbons. In both cases, up to 30 wt% UHMWPE could be achieved. Samples were prepared at 10, 15, 20, and 30 wt% loadings of UHMWPE in either LDPE or HDPE, corresponding to LDPE*x* or HDPE*x* (where *x* = 0–30) respectively.

It was immediately obvious from visual inspection of the LDPE/UHMWPE blends that significant macroscopic phase separation had occurred – particles of UHMWPE were visibly embedded within the LDPE matrix resulting in a grainy texture (Table S9†). Analysis by scanning electron microscopy shows UHMWPE particles around 66 μm in dimeter embedded in the LDPE matrix, but homogeneous HDPE/UHMWPE blends (Fig. 5c and f and S49–S51†). The presence of two distinct thermal phases was observed clearly by DSC (Fig. 5a and S45a†). The pure LDPE had a melting transition at 110 °C, and the LDPE/UHMWPE blends showed two transitions, one corresponding to LDPE and the other to UHMWPE at 131 °C. The high melting point peak grew relative to the low melting peak as the proportion of UHMWPE increased in the blends.

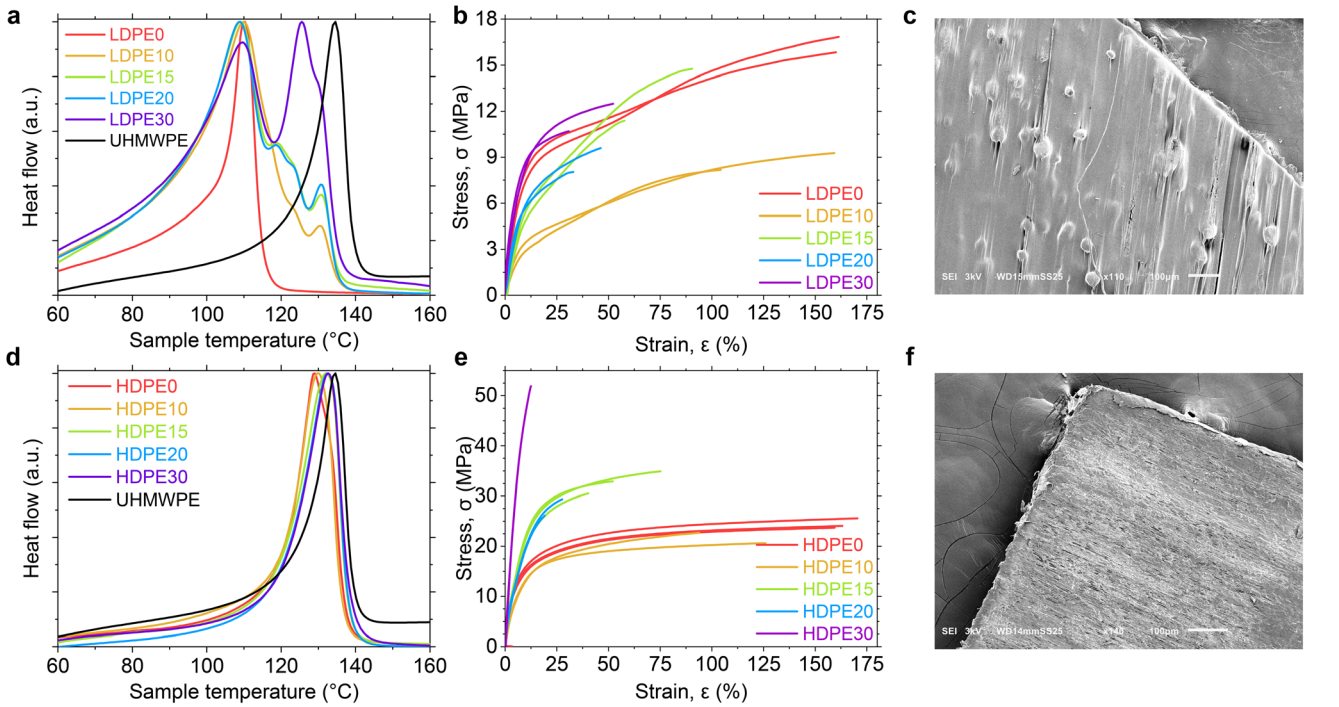

Fig. 5 (a and d) DSC thermograms (20 K min^{-1}, second heat), (b and e) engineering stress–strain curves (DMA force ramp) of LDPE/UHWMPE and HDPE/UHMWPE microcompounded blends across a composition range of 0–30 wt% UHMWPE; SEM images of LDPE/UHMWPE (c) and HDPE/UHMWPE (f) at 15 wt% UHMWPE.

Rheological characterisation of the melts shows that the complex viscosity, $|\eta^*|$, of LDPE/UHMWPE blends is at least two orders of magnitude less than the pure UHMWPE (Fig. S45c†). The viscosity curves are intermediate between that of the pure materials, in accordance with the law of mixtures, and appears consistent with melt-phase miscibility. This demonstrates that the melt processability advantages of the high MFI LDPE are maintained to an extent in the LDPE/UHMWPE blends. The solid-state viscoelastic properties of the LDPE/UHMWPE blends were studied by dynamic mechanical thermal analysis (DMTA) across a temperature range of −100 to +120 °C (Fig. S45d†). Two distinct β relaxation processes are observed with maxima in tan(δ) around −13 and 62 °C relating to the chain mobility of distinct thermal phases. The transition at −13 °C corresponds to chain mobility of the LDPE phase, while the transition at 62 °C, which is not present in LDPE0 (0 wt% UHMWPE), corresponds to the UHMWPE phase. The low-temperature subglass transition is coincident with the limit of the rubbery plateau, with flow-like behaviour emerging at increased temperatures as the LDPE chains become mobile. The mechanical properties of the LDPE/UHMWPE blends were investigated in the solid state by tensile analysis (Fig. 5b). Pure LDPE had a Young's modulus of 140 MPa, which decreased upon the addition of UHMWPE to 87.8 MPa for LDPE15 (15 wt% UHMWPE). In addition to the reduction in stiffness, the blends became more brittle than either of the pure polymers, with the fracture strain decreasing from 139% (LDPE0) to 53.7% (LDPE15). Moreover, the tensile strength of the blends also decreased from 16.8 MPa (LDPE0) to 12.5 MPa (LDPE30). The reduction in stiffness, ductility, and strength with increasing UHMWPE content is a result of the poor PE–PE miscibility and consequent phase separation, with stress concentrating at the UHMWPE grain boundaries. Despite good melt-flow properties and processability, the poor LDPE–UHMWPE miscibility means that the advantageous mechanical properties of UHMWPE are not conferred upon LDPE blends.

In contrast, blends based on an HDPE matrix appeared, at least superficially, homogeneous. A single thermal phase is observed by DSC, with the HDPE/UHMWPE blends having melting transition temperatures intermediate between that of the pure polymers, fulfilling the rule of mixtures (Fig. 5d). Peak broadening has been linked to the formation of separate crystals, which is not seen in this case.[98] This is evidence for good PE–PE miscibility between the two molecular weight grades, possibly aided by the chain explosion melting of nascent disentangled UHMWPE compensating for the typically extremely slow chain diffusion.[43] A less drastic reduction in complex viscosity was observed with HDPE than LDPE, as a result of the higher molecular weight and lower MFI. At high shear rates, the complex viscosities of the HDPE/UHMWPE samples converged (Fig. S46c†). However, at lower shear rates, the viscosity of HDPE30 is up to three orders of magnitude lower compared to UHMWPE. The formation of a fully miscible single thermal phase is confirmed by the presence of a single β transition in DMTA (Fig. S46d†). The HDPE0 transition is observed at 80 °C, while the β transition of the HDPE/UHMWPE blends appears instead at 100 °C. A slight maximum in tan(δ) at −60 °C for HDPE30 may indicate a deviation from ideal mixing at higher UHWMPE loadings. The rubbery plateau is maintained until 10 °C, after which a smooth transition to flow-like behaviour is observed. The mechanical properties of HDPE/UHMWPE blends are improved relative to HDPE0, with the Young's modulus increasing 71% from 425 to 726 MPa (HDPE0 and HDPE30 respectively), and the tensile strength increasing 103% from 25.6 to 51.9 MPa (HDPE0 and HDPE30 respectively; Fig. 5e). Unlike the nanostructured bimodal polymers produced by multisite catalysts *vide supra*, the mechanical properties of these blends follow simple mixing laws. The increase in strength and stiffness came at the expense of ductility however, with the strain at break decreasing from 171% to 12%. The significantly improved melt processability of HDPE/UHMWPE compared to pure UHMWPE, and the increase of strength, stiffness, and brittleness as a function of UHMWPE content shows that the desirable properties of both polymer components are maintained in the blend.

3 Conclusions

The synthesis and characterisation of ultra-high molecular weight polyethylene using heterogenised permethylindenylphenoxy (PHENI*) catalysts has been explored in detail. Four approaches to enhancing the processability of UHMWPE have been assessed: active site concentration and disentanglement; chain transfer agents; multisite catalysis; and polymer composites. It was found that below a critical surface concentration (at least 1%), further increases to disentanglement could not be observed. A strong hydrogen response was observed, with low molecular weight PE (85 kDa) produced at 2% H_2 concentration. Diethyl zinc proved to be an effective CTA, with sequential reactivity leading to broadened MWDs – including the production of bimodal polymer – and decreased melt viscosity. Coimmobilising complexes bearing PHENI* and EBI ligands on sMAO afforded multisite catalysts able to produce nanostructured bimodal polyethylene with desirable rheological and synergistic mechanical properties. Miscible blends of UHMWPE and HDPE resulted in effective reinforcement of the HDPE matrix, but LDPE was found to be immiscible. Using PHENI* catalysts, these approaches and combinations thereof are considered crucial to expanding the applicability of high-performance UHMW polymers. Moreover, combining chain shuttling polymerisation with multisite catalysis may enable the development of polyolefin block copolymers with novel properties utilising the exceptional comonomer affinity of PHENI*.[99,100]

4 Experimental

4.1 General procedures

Air- and moisture-sensitive compounds were manipulated under an inert atmosphere using standard Schlenk line techniques on a dual manifold vacuum/nitrogen line or in an

MBraun Labmaster 100 glovebox. Hexane and toluene were dried using an MBraun SPS 800 solvent purification system, stored over a potassium mirror and degassed under partial vacuum before use.

4.2 Gel-permeation chromatography

Gel-permeation chromatography was performed on a high temperature gel-permeation chromatograph with an IR5 infrared detector. Samples were prepared by dissolution in 1,2,4-trichlorobenzene (TCB) containing 300 ppm of 3,5-di-*tert*-butyl-4-hydroxytoluene (BHT) at 160 °C for 90 minutes and then filtered with a 10 μm SS filter before being passed through the GPC column. The samples were run under a flow rate of 0.5 mL min^{-1} using TCB containing 300 ppm BHT as mobile phase with 1 mg mL^{-1} BHT added as a flow rate marker. The GPC column and detector temperature were set at 145 and 160 °C respectively.

4.3 Differential scanning calorimetry

Differential scanning calorimetry was performed on a Perkin Elmer DSC 4000 system within a temperature range of 30–180 °C at a rate of 20 K min^{-1} unless otherwise stated. Polymer samples were sealed in 100 μL aluminium crucibles. An empty crucible was used as a reference and the DSC was calibrated using indium and zinc.

4.4 Rheometry

Rheometry was performed on a TA Instruments Discovery HR-2 hybrid rheometer using a temperature controlled stainless steel Peltier plate and a flat parallel plate geometry (20 mm diameter) with a working gap of 1000 μm. Approximately 200 mg of material, with *ca.* 0.1 wt% Irganox® 1010 was either vacuum compression moulded into a disc (10 mm diameter) at 180 °C or pelletised under a 15 ton force at ambient temperature. SAOS measurements were recorded at 160 °C under a flow of dry nitrogen in continuous oscillation (direct strain) mode at a strain of 0.1% (within the LVE region) and a logarithmic frequency sweep was performed from 0.01–100 rad s^{-1}. Data were processed using TRIOS®.

4.5 Dynamic mechanical analysis

Dynamic mechanical thermal analysis (DMTA) was performed on a TA Instruments Discovery HR-2 hybrid rheometer using the DMA mode (film tension) accessory. Approx. 150–200 mg of material was vacuum compression moulded into an ISO 37 type 3 dogbone (width b_1 = 4 mm, length L_0 = 10 mm, thickness *ca.* 1 mm) at 150–180 °C. Tensile properties were determined at ambient temperature using a sinusoidal frequency sweep (0.001–16 Hz) at 0.1% strain. DMTA of microcompounded films was performed on a TA Instruments Q800 DMA equipped with a TA Instruments ACS-3 chiller system. Rectangular samples were cut from extruded ribbons with a width of approx. 7 mm, thickness 50–500 μm, and length approx. 10 mm. Samples were fixed in a film clamp with 5 psi clamping force and subjected to a heating protocol from −100 to 125 °C at 3 K min^{-1} and a 1 Hz sinusoidal displacement applied at 0.1% strain. Force ramps were performed at room temperature on samples with width approx. 4 mm from 0 to 18 N at a rate of 0.25 N min^{-1} (for 50 μm thick films) with the rate scaled proportionally to the samples thickness to maintain a stress rate of approx. 1 MPa min^{-1}.

4.6 Microcompounding

UHMWPE was blended with either LDPE or HDPE inside a DSM Xplore 15 cc micro-compounder in recirculation mode for about 5 minutes using a screw speed of 100 rpm under an argon atmosphere. The temperature was set separately for the three zones: top (beginning of the screws/feeding area) 150–200 °C, middle 150–200 °C and bottom (tip of the screws/die area) 150–205 °C. After blending, the samples were collected in a ribbon using a flat film die. The take-off system consisted of an air blade positioned close to the die used for fast cooling to avoid or limit lateral shrinkage of the extruded material; a speed-controlled collection roll; and a torque-controlled winding roll.

4.7 Mechanical analysis

Mechanical analysis of UHMWPE was performed by first adding a thermal stabiliser (BHT)[101] and pressing into plates (80 × 60 × 1 mm) at 180–200 °C. Density was measured in triplicate at 23 °C according to ISO 1183-1 (2012) on a Mettler Toledo XS204 instrument. Tensile properties were determined in quintuplicate at 23 °C according to ISO 527-1/2 using type 5A test specimens on a Zwick Z010 instrument with a 5 kN load cell. The gauge length was L_0 = 20 mm, the gripping distance was L = 50 mm, and the testing speed was 50 mm min^{-1}. Bimodal PE synthesised by multisite catalysts was prepared by vacuum compression moulding into an ISO 37 Type 3 dogbone (width b_1 = 4 mm, length L_0 = 10 mm, thickness *ca.* 0.8 mm) at 180–200 °C. Before measurements, samples were conditioned for 7 days at room temperature. The measurements were performed using an Instron 5582 universal testing instrument equipped with a 5 kN load cell. A grip-to-grip separation of 40 mm was used. The samples were pre-stressed to 3 N, then loaded with a constant crosshead speed 100 mm min^{-1}. The reported values are an average of at least 4 consistent measurements of each.

4.8 Optical microscopy

Optical microscopy was performed using a Leica M205 C encoded stereo microscope.

4.9 Scanning electron microscopy

Scanning electron microscopy (SEM) images were collected on a JEOL JSM-6010LV scanning electron microscope. Samples were prepared on carbon tape and coated with Au/Pd using a Quorum Technologies SC7620 sputter coater to reduce charge buildup and improve image quality.

4.10 Wide angle X-ray scattering

Wide angle X-ray scattering (WAXS) was performed using a PANalytical X'Pert Pro diffractometer in scanning mode, using Cu Kα radiation (λ = 1.540598 Å, λ_{α_2} = 1.544426 Å, α_1/α_2 = 0.5) at 40 kV and 20 mA. Samples were mounted on stainless steel or silicon sample holders and scans were recorded from 10° ≤ 2θ ≤ 60° with a step size of 0.016711° and 60 s per step unless indicated otherwise.

4.11 Commercially supplied materials and literature preparations

PHENI* complex **1** was synthesised according to a literature procedure.[52] LDPE, Irganox® 1010, tri*iso*butyl aluminium, *rac*-EBIZrCl$_2$ (Sigma Aldrich), and HDPE (SCG Chemicals PLC) were all used as received. Ethylene was supplied by BOC Ltd. and was passed through pre-activated molecular sieves before use. Ethylene/hydrogen was supplied by BUSE Scientific Ltd. and used as received. Solid polymethylaluminoxane (sMAO, third generation) was supplied by SCG Chemicals PLC as a slurry in toluene and was dried under vacuum before use.

4.12 Preparation of supported catalysts

In a typical immobilisation procedure, sMAO (250 mg) and the precatalyst ([Al$_{sMAO}$]/[Ti] = 200) were weighed into a Schlenk flask. Toluene (40 mL) was added and the slurry was heated at 60 °C with regular swirling for 1 h or until the supernatant had discoloured. The coloured solid was allowed to settle, then the supernatant was decanted and the solid product dried under vacuum at room temperature (1×10^{-2} mbar).

4.13 Polymerisation of ethylene

In a typical polymerisation reaction, a 150 mL Rotaflo® ampoule with a magnetic stir bar was charged with TIBA (150 mg), solid catalyst (10 mg), and hexanes (50 mL). The ampoule was sealed, cycled onto a Schlenk line and the headspace degassed under reduced pressure. The Schlenk line was cycled a further two times using ethylene as the purge gas while the vessel was brought to temperature in a thermostatic oil bath with the stirring set at 1000 rpm. The stopcock was opened to ethylene at a pressure of 2 bar and the timer was started. After 30 minutes the vessel was degassed under partial vacuum, the polymer was collected by filtration through a sintered glass frit (porosity 3), and washed with 2 × 25 mL pentane. The polyethylene was dried under vacuum until constant weight. All runs were carried out at least in duplicate.

Data availability

The data supporting this article have been included as part of the ESI.†

Author contributions

C. G. C. R. – conceptualisation, investigation, writing – original draft, review and editing, funding acquisition. A. E. – investigation. Z. R. T. – conceptualisation, supervision, writing – review and editing. J. W. – conceptualisation, project administration. D. O'H. – conceptualisation, supervision, funding acquisition. All authors have read and approved the final manuscript.

Conflicts of interest

There are no competing financial conflicts to declare.

Acknowledgements

C. G. C. R., A. E., and Z. R. T. would like to thank SCG Chemicals PLC for financial support. C. G. C. R. additionally acknowledges funding from the Engineering and Physical Sciences Research Council Impact Acceleration Account (EP/X525777/1). The authors thank Liv Thobru, Sara R. Herum, Rita Jenssen, and David Laursen (Norner AS, Norway) for GPC analysis; Thea H. Glittum and Heidi N. Bryntesen (Norner AS, Norway) for mechanical testing; Giovanni Santagiuliana and Philip Kennedy (Nanoforce Technology Ltd.) for microcompounding; and Nick Hawkins (University of Oxford) for assistance with DMTA.

References

1 J. M. Kelly, Ultra-high molecular weight polyethylene, *J. Macromol. Sci., Polym. Rev.*, 2002, **42**, 355–371.
2 K. Patel, S. H. Chikkali and S. Sivaram, Ultrahigh molecular weight polyethylene: Catalysis, structure, properties, processing and applications, *Prog. Polym. Sci.*, 2020, **109**, 101290.
3 J. Fu, B. W. Ghali, A. J. Lozynsky, E. Oral and O. K. Muratoglu, Ultra high molecular weight polyethylene with improved plasticity and toughness by high temperature melting, *Polymer*, 2010, **51**, 2721–2731.
4 T. A. Tervoort, J. Visjager and P. Smith, On abrasive wear of polyethylene, *Macromolecules*, 2002, **35**, 8467–8471.
5 P. Bracco, A. Bellare, A. Bistolfi and S. Affatato, Ultra-high molecular weight polyethylene: Influence of the chemical, physical and mechanical properties on the wear behavior. A review, *Materials*, 2017, **10**, 791.
6 F. Živić, M. Babić, S. Mitrović, D. Adamović and S. Pelemis, Friction coefficient of UHMWPE during dry reciprocating sliding, *Tribol. Ind.*, 2014, **36**, 281.
7 S. Rastogi, Y. Yao, S. Ronca, J. Bos and J. van der Eem, Unprecedented high-modulus high-strength tapes and films of ultrahigh molecular weight polyethylene via solvent-free route, *Macromolecules*, 2011, **44**, 5558–5568.
8 M. Hussain, R. A. Naqvi, N. Abbas, S. M. Khan, S. Nawaz, A. Hussain, N. Zahra and M. W. Khalid, Ultra-high-molecular-weight-polyethylene (UHMWPE) as a promising polymer material for biomedical applications: A concise review, *Polymers*, 2020, **12**, 323.

9 Y. Wang and R. Hou, Research progress on surface modification and application status of UHMWPE fiber, *J. Phys.: Conf. Ser.*, 2022, **2263**, 012016.
10 S. Liu, J. Wang, Y. Wang and Y. Wang, Improving the ballistic performance of ultra high molecular weight polyethylene fiber reinforced composites using conch particles, *Mater. Des.*, 2010, **31**, 1711–1715.
11 D. Romano, S. Ronca and S. Rastogi, A hemi-metallocene chromium catalyst with trimethylaluminum-free methylaluminoxane for the synthesis of disentangled ultra-high molecular weight polyethylene, *Macromol. Rapid Commun.*, 2015, **36**, 327–331.
12 E. M. Brach del Prever, A. Bistolfi, P. Bracco and L. Costa, UHMWPE for arthroplasty: Past or future?, *J. Orthop. Traumatol.*, 2009, **10**, 1–8.
13 S. Santavirta, Y. T. Konttinen, R. Lappalainen, A. Anttila, S. B. Goodman, M. Lind, L. Smith, M. Takagi, E. Gómez-Barrena, L. Nordsletten and J. W. Xu, Materials in total joint replacement, *Curr. Orthop.*, 1998, **12**, 51–57.
14 F. P. Zaribaf, Medical-grade ultra-high molecular weight polyethylene: Past, current and future, *Mater. Sci. Technol.*, 2018, **34**, 1940–1953.
15 M. Cao, L. Chen, R. Xu and Q. Fang, Effect of the temperature on ballistic performance of UHMWPE laminate with limited thickness, *Compos. Struct.*, 2021, **277**, 114638.
16 H. Wang, D. Weerasinghe, D. Mohotti, P. J. Hazell, V. P. W. Shim, K. Shankar and E. V. Morozov, On the impact response of UHMWPE woven fabrics: Experiments and simulations, *Int. J. Mech. Sci.*, 2021, **204**, 106574.
17 C. J. Kuo and W. L. Lan, in *Advances in filament yarn spinning of textiles and polymers*, ed. D. Zhang, Woodhead Publishing, 2014, pp. 100–112.
18 S. Chhetri and H. Bougherara, A comprehensive review on surface modification of UHMWPE fiber and interfacial properties, *Composites, Part A*, 2021, **140**, 106146.
19 X. Zhuang and X. Yan, Investigation of damage mechanisms in self-reinforced polyethylene composites by acoustic emission, *Compos. Sci. Technol.*, 2006, **66**, 444–449.
20 X. Zhang, Y. Wang, C. Lu and S. Cheng, Interfacial adhesion study on UHMWPE fiber-reinforced composites, *Polym. Bull.*, 2011, **67**, 527–540.
21 M. Mihailov and L. Minkova, Pecularities of the thermomechanical behaviour of ultra-high molecular weight linear polyethylene and its blends with linear polyethylene of normal molecular weight, *Colloid Polym. Sci.*, 1987, **265**, 681–685.
22 D. Shelly, S.-Y. Lee and S.-J. Park, Compatibilization of ultra-high molecular weight polyethylene (UHMWPE) fibers and their composites for superior mechanical performance: A concise review, *Composites, Part B*, 2024, **275**, 111294.
23 A. Pandey, Y. Champouret and S. Rastogi, Heterogeneity in the distribution of entanglement density during polymerization in disentangled ultrahigh molecular weight polyethylene, *Macromolecules*, 2011, **44**, 4952–4960.
24 X. Tang, J. H. Xing, X. Yan, C. L. Ye, L. T. Zhang, Y. Zhang, B. Q. Shu, J. S. Mu, W. Li, J. D. Wang and Y. R. Yang, Metallocene polyolefins reinforced by low-entanglement UHMWPE through interfacial entanglements, *Adv. Polym. Technol.*, 2022, **2022**, 9344096.
25 Z. Bartczak, Effect of chain entanglements on plastic deformation behavior of ultra-high molecular weight polyethylene, *J. Polym. Sci., Part B: Polym. Phys.*, 2010, **48**, 276–285.
26 S. Rastogi, D. R. Lippits, G. W. M. Peters, R. Graf, Y. Yao and H. W. Spiess, Heterogeneity in polymer melts from melting of polymer crystals, *Nat. Mater.*, 2005, **4**, 635–641.
27 R. Edgeworth, B. J. Dalton and T. Parnell, The pitch drop experiment, *Eur. J. Phys.*, 1984, **5**, 198.
28 D. Romano, N. Tops, E. Andablo-Reyes, S. Ronca and S. Rastogi, Influence of polymerization conditions on melting kinetics of low entangled UHMWPE and its implications on mechanical properties, *Macromolecules*, 2014, **47**, 4750–4760.
29 B. Wu, Y. Cai, X. Zhao and L. Ye, Fabrication of well-miscible and highly enhanced polyethylene/ultrahigh molecular weight polyethylene blends by facile construction of interfacial intermolecular entanglement, *Polym. Test.*, 2021, **93**, 106973.
30 M. Stürzel, T. Hees, M. Enders, Y. Thomann, H. Blattmann and R. Mülhaupt, Nanostructured polyethylene reactor blends with tailored trimodal molar mass distributions as melt-processable all-polymer composites, *Macromolecules*, 2016, **49**, 8048–8060.
31 Z. Yue, N. Wang, Y. Cao, W. Li and C. D. Dong, Reduced entanglement density of ultrahigh-molecular-weight polyethylene favored by the isolated immobilization on the $MgCl_2$ (110) plane, *Ind. Eng. Chem. Res.*, 2020, **59**, 3351–3358.
32 M. Chen, Y. Chen, W. Li, P. Liang, C. Ren, B. Jiang, J. Wang and Y. Yang, Synthesis of weakly entangled ultra-high-molecular-weight polyethylene with a fine particle size, *Ind. Eng. Chem. Res.*, 2021, **60**, 3354–3362.
33 P. Chammingkwan, Y. Bando, L. T. T. Mai, T. Wada, A. Thakur, M. Terano, L. Sinthusai and T. Taniike, Less entangled ultrahigh-molecular-weight polyethylene produced by nano-dispersed Ziegler–Natta catalyst, *Ind. Eng. Chem. Res.*, 2021, **60**, 2818–2827.
34 R. P. Gote, D. Mandal, K. Patel, K. Chaudhuri, C. P. Vinod, A. K. Lele and S. H. Chikkali, Judicious reduction of supported Ti catalyst enables access to disentangled ultrahigh molecular weight polyethylene, *Macromolecules*, 2018, **51**, 4541–4552.
35 J. Dai, C. Yu, S. Ye, W. Li, X. Kang, Y. Yang, P. Liang, Y. Ma, Z. Huang, B. Jiang, J. Wang and Y. Yang, The intermittent dormancy of ethylene polymerization with the assistance of nitrogen microbubbles, *Macromolecules*, 2021, **54**, 9418–9426.
36 S. Ye, J. Dai, W. Li, Y. Yang, Z. Huang, J. Wang and Y. Yang, Tailoring the chain entanglement by nitrogen bubble-assisted polymerization, *Ind. Eng. Chem. Res.*, 2021, **60**, 15951–15959.

37 A. A. Antonov and K. P. Bryliakov, Post-metallocene catalysts for the synthesis of ultrahigh molecular weight polyethylene: Recent advances, *Eur. Polym. J.*, 2021, **142**, 110162.
38 D. Romano, E. Andablo-Reyes, S. Ronca and S. Rastogi, Aluminoxane co-catalysts for the activation of a bis phenoxyimine titanium (IV) catalyst in the synthesis of disentangled ultra-high molecular weight polyethylene, *Polymer*, 2015, **74**, 76–85.
39 G. Forte and S. Ronca, Synthesis of disentangled ultra-high molecular weight polyethylene: Influence of reaction medium on material properties, *Int. J. Polym. Sci.*, 2017, **2017**, 1–8.
40 M. Spronck, A. Klein, B. Blom and D. Romano, Synthesis of disentangled ultra-high molecular weight polyethylene using vanadium(V)-based catalysts, *Z. Anorg. Allg. Chem.*, 2018, **644**, 993–998.
41 I. V. Oleynik, I. K. Shundrina and I. I. Oleyinik, Highly active titanium (IV) dichloride FI catalysts bearing a diallylamino group for the synthesis of disentangled UHMWPE, *Polym. Adv. Technol.*, 2020, **31**, 1921–1934.
42 Z. Zhang, X. Kang, Y. Jiang, Z. Cai, S. Li and D. Cui, Access to disentangled ultrahigh molecular weight polyethylene via a binuclear synergic effect, *Angew. Chem., Int. Ed.*, 2023, **62**, e202215582.
43 F. Christakopoulos, E. Troisi, N. Friederichs, J. Vermant and T. A. Tervoort, "Tying the knot": Enhanced recycling through ultrafast entangling across ultrahigh molecular weight polyethylene interfaces, *Macromolecules*, 2021, **54**, 9452–9460.
44 D. T. Gentekos, R. J. Sifri and B. P. Fors, Controlling polymer properties through the shape of the molecular-weight distribution, *Nat. Rev. Mater.*, 2019, **4**, 761–774.
45 Y. Zhao, L. Wang, H. Yu, G. Jing, C. Li, Y. Chen and M. Saleem, Facile preparation of bimodal polyethylene with tunable molecular weight distribution from ethylene polymerization catalyzed by binary catalytic system in the presence of diethyl zinc, *J. Polym. Res.*, 2014, **21**, 470.
46 C. Zou, S. Dai and C. Chen, Ethylene polymerization and copolymerization using nickel 2-iminopyridine-N-oxide catalysts: Modulation of polymer molecular weights and molecular-weight distributions, *Macromolecules*, 2018, **51**, 49–56.
47 T. Kida, R. Tanaka, Y. Hiejima, K. H. Nitta and T. Shiono, Improving the strength of polyethylene solids by simple controlling of the molecular weight distribution, *Polymer*, 2021, **218**, 123526.
48 M. Stürzel, S. Mihan and R. Mülhaupt, From multisite polymerization catalysis to sustainable materials and all-polyolefin composites, *Chem. Rev.*, 2016, **116**, 1398–1433.
49 T. K. Han, H. K. Choi, D. W. Jeung, Y. S. Ko and S. I. Woo, Control of molecular weight and molecular weight distribution in ethylene polymerization with metallocene catalysts, *Macromol. Chem. Phys.*, 1995, **196**, 2637–2647.
50 C. Long, Z. Dong, X. Liu, F. Yu, Y. Shang, K. Wang, S. Feng, X. Hou, C. He and Z. R. Chen, Simultaneous enhancement in processability and mechanical properties of polyethylenes via tuning the molecular weight distribution from unimodal to bimodal shape, *Polymer*, 2022, **258**, 125287.
51 P. Kenyon, D. W. J. Leung, Z. R. Turner, J.-C. Buffet and D. O'Hare, Tuning polyethylene molecular weight distributions using catalyst support composition, *Macromolecules*, 2022, **55**, 3408–3414.
52 C. G. Collins Rice, J.-C. Buffet, Z. R. Turner and D. O'Hare, Supported permethylindenyl titanium catalysts for the synthesis of disentangled ultra-high molecular weight polyethylene (disUHMWPE), *Chem. Commun.*, 2021, **57**, 8600–8603.
53 C. G. Collins Rice, J.-C. Buffet, Z. R. Turner and D. O'Hare, Efficient synthesis of thermoplastic elastomeric amorphous ultra-high molecular weight atactic polypropylene (UHMWaPP), *Polym. Chem.*, 2022, **13**, 5597–5603.
54 C. G. Collins Rice, J. A. Hayden, A. D. Hawkins, L. J. Morris, Z. R. Turner, J.-C. Buffet and D. O'Hare, Trends in structure and ethylene polymerization reactivity of transition-metal permethylindenyl-phenoxy (PHENI*) complexes, *Organometallics*, 2024, **43**, 540–556.
55 S. Rastogi, Y. Yao, D. R. Lippits, G. W. H. Höhne, R. Graf, H. W. Spiess and P. J. Lemstra, Segmental mobility in the non-crystalline regions of semicrystalline polymers and its implications on melting, *Macromol. Rapid Commun.*, 2009, **30**, 826–839.
56 D. R. Lippits, S. Rastogi, G. W. H. Höhne, B. Mezari and P. C. M. M. Magusin, Heterogeneous distribution of entanglements in the polymer melt and its influence on crystallization, *Macromolecules*, 2007, **40**, 1004–1010.
57 N. Li, Q. Zhang, Q. Yang, Y. Huang, X. Liao and W. Zhao, The dependence time of melting behavior on rheological aspects of disentangled polymer melt: A route to the heterogeneous melt, *J. Polym. Res.*, 2015, **22**, 55.
58 J. D. Ferry, *Viscoelastic properties of polymers*, John Wiley & Sons, 1980.
59 A. Pandey, A. Toda and S. Rastogi, Influence of amorphous component on melting of semicrystalline polymers, *Macromolecules*, 2011, **44**, 8042–8055.
60 J. D. Kim, J. B. P. Soares and G. L. Rempel, Use of hydrogen for the tailoring of the molecular weight distribution of polyethylene in a bimetallic supported metallocene catalyst system, *Macromol. Rapid Commun.*, 1998, **19**, 197–199.
61 M. I. Nikolaeva, T. B. Mikenas, M. A. Matsko, L. G. Echevskaya and V. A. Zakharov, Ethylene polymerization over supported titanium-magnesium catalysts: Effect of polymerization parameters on the molecular weight distribution of polyethylene, *J. Appl. Polym. Sci.*, 2011, **122**, 3092–3101.
62 T. C. Chung, G. Xu, Y. Lu and Y. Hu, Metallocene-mediated olefin polymerization with B–H chain transfer agents: Synthesis of chain-end functionalized polyolefins and diblock copolymers, *Macromolecules*, 2001, **34**, 8040–8050.
63 W. Wang, L. Hou, T. Zhang and C. Liu, Chain transfer reaction to diethylzinc in ethylene polymerization by metallocene catalysts, *J. Polym. Res.*, 2018, **25**, 145.

64 R. Blom and I. M. Dahl, On the sensitivity of metallocene catalysts toward molecular hydrogen during ethylene polymerization, *Macromol. Chem. Phys.*, 1999, **200**, 442–449.
65 Y. V. Kissin and A. S. Goldman, Chemistry and mechanism of alkene polymerization reactions with metallocene catalysts, *Macromol. Chem. Phys.*, 2009, **210**, 1942–1956.
66 J. Ramos, V. Cruz, A. Muñoz-Escalona and J. Martínez-Salazar, Ab initio study of hydrogenolysis as a chain transfer mechanism in olefin polymerization catalyzed by metallocenes, *Polymer*, 2000, **41**, 6161–6169.
67 W. Kaminsky and H. Lüker, Influence of hydrogen on the polymerization of ethylene with the homogeneous Ziegler system bis(cyclopentadienyl)zirconiumdichloride/aluminoxane, *Makromol. Chem., Rapid Commun.*, 1984, **5**, 225–228.
68 Y. V. Kissin, R. I. Mink, T. E. Nowlin and A. J. Brandolini, Ethylene polymerization reactions with Ziegler–Natta catalysts. III. Chain-end structures and polymerization mechanism, *J. Polym. Sci., Part A: Polym. Chem.*, 1999, **37**, 4281–4294.
69 K. J. Chu, J. B. P. Soares and A. Penlidis, Effect of hydrogen on ethylene polymerization using in-situ supported metallocene catalysts, *Macromol. Chem. Phys.*, 2000, **201**, 552–557.
70 A. K. Rappé, W. M. Skiff and C. J. Casewit, Modeling metal-catalyzed olefin polymerization, *Chem. Rev.*, 2000, **100**, 1435–1456.
71 F. Song, R. D. Cannon, S. J. Lancaster and M. Bochmann, Activator effects in metallocene-based alkene polymerisations: Unexpectedly strong dependence of catalyst activity on trityl concentration, *J. Mol. Catal. A: Chem.*, 2004, **218**, 21–28.
72 M. Bochmann, The chemistry of catalyst activation: The case of group 4 polymerization catalysts, *Organometallics*, 2010, **29**, 4711–4740.
73 K. Wang, Y. Gao, J. Yi, N. Zhao, Y. Jin, X. He and B. Liu, Study of silica-supported chromocene catalysts for ethylene polymerization, *Macromol. Chem. Phys.*, 2020, **221**, 2000181.
74 L. G. Echevskaya, M. A. Matsko, T. B. Mikenas, V. E. Nikitin and V. A. Zakharov, Supported titanium–magnesium catalysts with different titanium content: Kinetic peculiarities at ethylene homopolymerization and copolymerization and molecular weight characteristics of polyethylene, *J. Appl. Polym. Sci.*, 2006, **102**, 5436–5442.
75 M. A. Matsko, M. I. Nikolaeva and V. A. Zakharov, Hydrogen effect on the molecular weight distribution of polymers obtained by polymerization of ethylene and α-olefins over supported titanium-magnesium catalysts, *J. Appl. Polym. Sci.*, 2021, **138**, 50256.
76 T. J. Williams, J. V. Lamb, J.-C. Buffet, T. Khamnaen and D. O'Hare, Synthesis of ultra-high molecular weight poly(ethylene)-co-(1-hexene) copolymers through high-throughput catalyst screening, *RSC Adv.*, 2021, **11**, 5644–5650.
77 J. V. Lamb, J.-C. Buffet, Z. R. Turner, T. Khamnaen and D. O'Hare, Metallocene polyethylene wax synthesis, *Macromolecules*, 2020, **53**, 5847–5856.
78 H. J. Lee, J. W. Baek, T. J. Kim, H. S. Park, S. H. Moon, K. L. Park, S. M. Bae, J. Park and B. Y. Lee, Synthesis of long-chain branched polyolefins by coordinative chain transfer polymerization, *Macromolecules*, 2019, **52**, 9311–9320.
79 L. Boggioni, D. Sidari, S. Losio, U. M. Stehling, F. Auriemma, R. Di Girolamo, C. De Rosa and I. Tritto, Ethylene–co–norbornene copolymerization in the presence of a chain transfer agent, *Eur. Polym. J.*, 2018, **107**, 54–66.
80 W. Liu, S. Guo, Z. Bu, H. Fan, W.-J. Wang and B.-G. Li, Synthesis of molecular weight controllable bimodal polyethylene from fluorinated FI–Ti catalyst coupled with $ZnEt_2$, *Eur. Polym. J.*, 2013, **49**, 1823–1831.
81 D. J. Arriola, E. M. Carnahan, P. D. Hustad, R. L. Kuhlman and T. T. Wenzel, Catalytic production of olefin block copolymers via chain shuttling polymerization, *Science*, 2006, **312**, 714–719.
82 M. Sun, Y. Xiao, K. Liu, X. Yang, P. Liu, S. Jie, J. Hu, S. Shi, Q. Wang, K. H. Lim, Z. Liu, B.-G. Li and W.-J. Wang, Synthesis and characterization of polyolefin thermoplastic elastomers: A review, *Can. J. Chem. Eng.*, 2023, **101**, 4886–4906.
83 L. Sun, E. Szuromi, T. Karjala, Z. Zhou and E. Carnahan, Synthesis of chain shuttling organometallic compounds capable of producing triblock polyolefins, *Macromolecules*, 2020, **53**, 10796–10802.
84 E. Karaagac, T. Koch and V.-M. Archodoulaki, Choosing an effective compatibilizer for a virgin HDPE rich-HDPE/PP model blend, *Polymers*, 2021, **13**, 3567.
85 S. G. M. Périn, J. R. Severn, C. E. Koning and J. C. Chadwick, Unusual effect of diethyl zinc and triisobutylaluminium in ethylene/1-hexene copolymerisation using an $MgCl_2$-supported Ziegler-Natta catalyst, *Macromol. Chem. Phys.*, 2006, **207**, 50–56.
86 D. W. Mead, Determination of molecular weight distributions of linear flexible polymers from linear viscoelastic material functions, *J. Rheol.*, 1994, **38**, 1797–1827.
87 A. Kurek, S. Mark, M. Enders, M. O. Kristen and R. Mülhaupt, Mesoporous silica supported multiple single-site catalysts and polyethylene reactor blends with tailor-made trimodal and ultra-broad molecular weight distributions, *Macromol. Rapid Commun.*, 2010, **31**, 1359–1363.
88 J. Moreno, R. van Grieken, A. Carrero and B. Paredes, Development of novel chromium oxide/metallocene hybrid catalysts for bimodal polyethylene, *Polymer*, 2011, **52**, 1891–1899.
89 M. Stürzel, A. G. Kurek, T. Hees, Y. Thomann, H. Blattmann and R. Mülhaupt, Multisite catalyst mediated polymer nanostructure formation and self-reinforced polyethylene reactor blends with improved toughness/stiffness balance, *Polymer*, 2016, **102**, 112–118.
90 A. B. Boscoletto, R. Franco, M. Scapin and M. Tavan, An investigation on rheological and impact behaviour of high density and ultra high molecular weight polyethylene mixtures, *Eur. Polym. J.*, 1997, **33**, 97–105.

91 Y. Chen, H. Zou, Y. Cao and M. Liang, Melt miscibility of HDPE/UHMWPE, LDPE/UHMWPE, and LLDPE/UHMWPE blends detected by dynamic rheometer, *Polym. Sci., Ser. A*, 2014, **56**, 630–639.
92 Y. Chen, H. Zou, M. Liang and P. Liu, Rheological, thermal, and morphological properties of low-density polyethylene/ultra-high-molecular-weight polyethylene and linear low-density polyethylene/ultra-high-molecular-weight polyethylene blends, *J. Appl. Polym. Sci.*, 2013, **129**, 945–953.
93 T. Kyu and P. Vadhar, Cocrystallization and miscibility studies of blends of ultrahigh molecular weight polyethylene with conventional polyethylenes, *J. Appl. Polym. Sci.*, 1986, **32**, 5575–5584.
94 L. Zhao and P. Choi, A review of the miscibility of polyethylene blends, *Mater. Manuf. Processes*, 2006, **21**, 135–142.
95 B. Crist and M. J. Hill, Recent developments in phase separation of polyolefin melt blends, *J. Polym. Sci., Part B: Polym. Phys.*, 1997, **35**, 2329–2353.
96 G. Tao, Y. Chen, J. Mu, L. Zhang, C. Ye and W. Li, Exploring the entangled state and molecular weight of UHMWPE on the microstructure and mechanical properties of HDPE/UHMWPE blends, *J. Appl. Polym. Sci.*, 2021, **138**, 50741.
97 K. Chaudhuri and A. K. Lele, Rheological quantification of the extent of dissolution of ultrahigh molecular weight polyethylene in melt-compounded blends with high density polyethylene, *J. Rheol.*, 2020, **64**, 1–12.
98 S. S. Khasraghi and M. Rezaei, Preparation and characterization of UHMWPE/HDPE/MWCNT melt-blended nanocomposites, *J. Thermoplast. Compos. Mater.*, 2015, **28**, 305–326.
99 C. G. Collins Rice, L. J. Morris, J.-C. Buffet, Z. R. Turner and D. O'Hare, Fully tuneable ethylene–propylene elastomers using a supported permethylindenyl-phenoxy (PHENI*) catalyst, *Chem. Commun.*, 2023, **59**, 12128–12131.
100 C. G. Collins Rice, L. J. Morris, J.-C. Buffet, Z. R. Turner and D. O'Hare, Towards designer polyolefins: Highly tuneable olefin copolymerisation using a single permethylindenyl post-metallocene catalyst, *Chem. Sci.*, 2023, **15**, 250–258.
101 P. P. Klemchuk and P. L. Horng, Perspectives on the stabilization of hydrocarbon polymers against thermo-oxidative degradation, *Polym. Degrad. Stab.*, 1984, **7**, 131–151.